Letter

Role of Metal−Chloride Anions in Photoluminescence Regulations for Hybrid Metal Halides

Binbin Su,[#] Gaomin Song,[#] Maxim S. Molokeev, Nicolay N. Golovnev, Maxim K. Lesnikov, Zheshuai Lin, and Zhiguo Xia*

Read Online

ACCESS | Metrics & More | Article Recommendations | SI Supporting Information

ABSTRACT: Organic−inorganic hybrid metal halides with emissive organic cations are of great interest due to their structural diversity and interesting photophysical properties. Here, we assemble emissive organic cations ($EnrofloH_2^{2+}$) with different metal−chloride anions ($Pb_2Cl_6^{2-}$ to $Bi_2Cl_{10}^{4-}$ to $SnCl_6^{2-}$) to form the new single crystal phases, and thus the photoluminescence properties of the metal halides, including Stokes shift, full width at half-maximum (FWHM), and photoluminescence quantum yield (PLQY) have been studied accordingly. ($EnrofloH_2$)$SnCl_6 \cdot H_2O$, as an example, possesses narrow FWHM and high PLQY, which are caused by the strong $\pi-\pi$ stacking and inter- and intramolecular hydrogen bonds interactions. Compared with $EnrofloH_2^{2+}$ cation in solution, the interactions generate a restraining effect and increase the rigid degree of $EnrofloH_2^{2+}$ cation in the bulk single crystals. Our work clarifies the photophysical properties of the $EnrofloH_2^{2+}$ organic cations by constructing the inter- and intramolecular interactions and boosts the further study of organic−inorganic hybrid metal halides materials with different luminescence mechanisms.
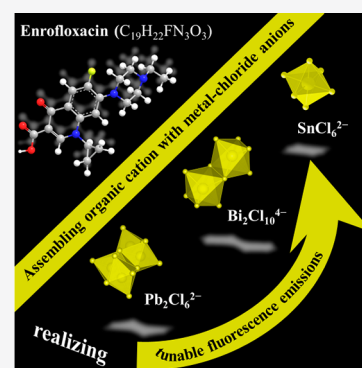
There has been a great development of organic−inorganic hybrid metal halides due to their unique advantages, such as solution-process, low cost, large-area production, and various applications.[1−3] The flexible selectivity of organic cations and center metal ions (Cu^+, Pb^{2+}, Sn^{2+}, Ge^{2+}, Bi^{3+}, Sn^{4+}, etc.) in these compounds allows a wide choice of the compositions for elements in achieving the desired properties for photonic applications, such as photovoltaic cells, photodetectors and light-emitting diodes (LEDs).[4−7] In general, the organic cations are divided into emissive organic cations and nonemissive organic cations according to the effect of organic cations on the photoluminescence (PL) behaviors of hybrid metal halides. The nonemissive organic cations only have a contribution to the construction of crystal structure for metal halides. In contrast, the emissive organic cations not only play a role in constructing the crystal structure but also have a contribution to the PL. Generally, luminescent metal halides exhibit free excitons (FEs) emission and self-trapped excitons (STEs) emission, related to the bandgap and the degree of lattice distortion for metal−halogen anions, which are found both in nonemissive and in emissive organic cation-containing compounds.[8−10] Especially, metal halides with emissive organic cations have flexible selectivity, and their PL comes from either the individual organic cations or the combination of the organic cations and STEs.[11−13]

Moreover, the emission of individual organic cations can be also regulated by selecting different metal−halogen anions.[14,15] As a result, reasonably assembling organic cations with metal−halogen anions to form the single crystals can alter the

luminescence properties of hybrid metal halide materials for future burgeoning optoelectronic applications.

Enrofloxacin, as an emissive organic molecule, is composed of the piperazinyl and quinoline groups (Figure 1). They can
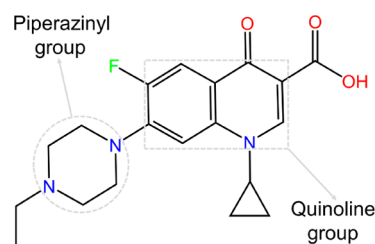

Figure 1. Chemical structure of Enrofloxacin (Enroflo).

be assembled with metal−halogen anions to form both complexes and ionic compounds.[16] Furthermore, the Enrofloxacin molecule can exist as cationic, zwitterionic, and anionic species in solution on the basis of different pH conditions, whose emissions are closely related to the degree of protonation.[17−20] In addition, their PL also can be controlled
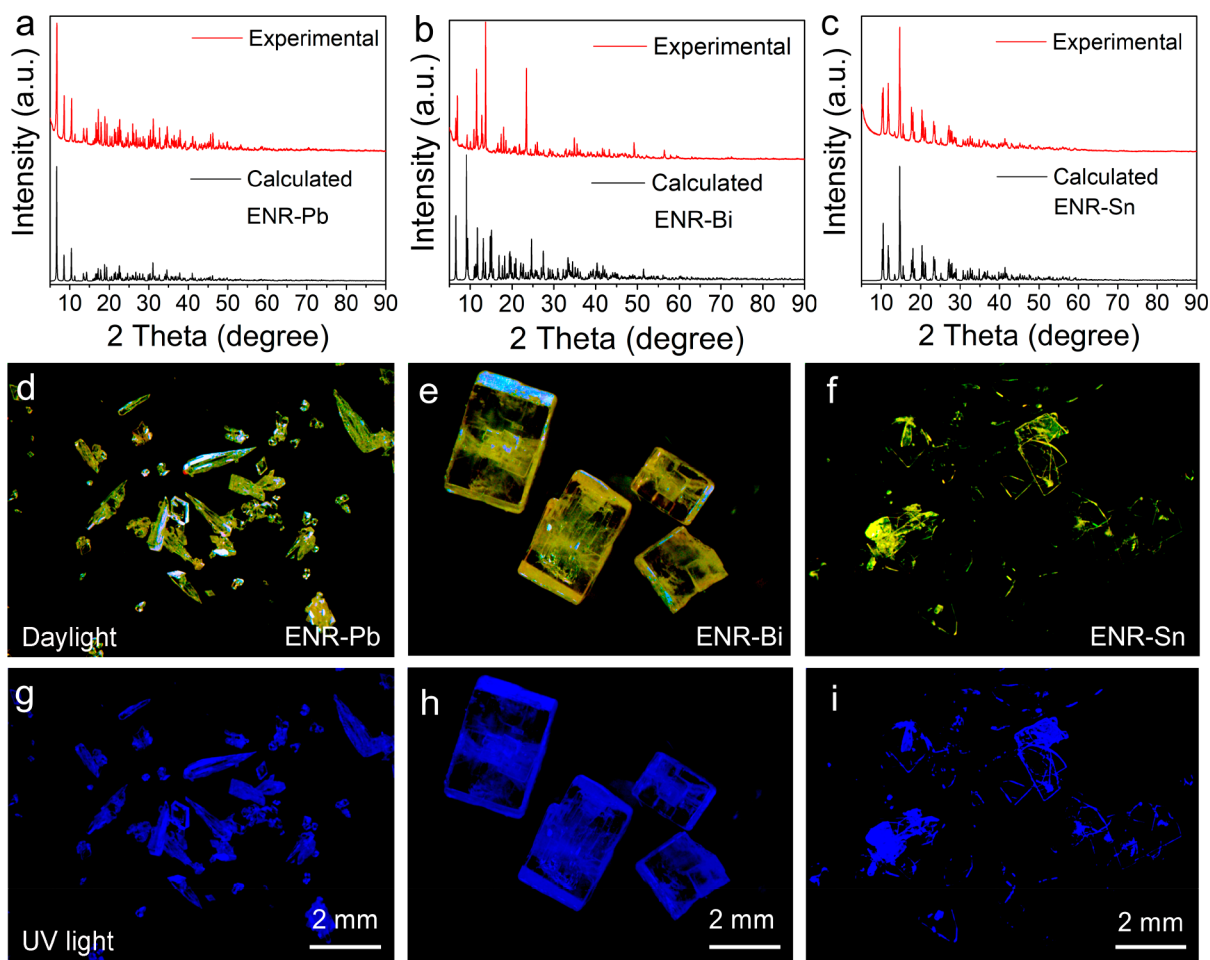
Figure 2. Calculated and experimental X-ray powder patterns of ENR-Pb (a), ENR-Bi (b), and ENR-Sn (c) crystals. Optical microscopic images of ENR-Pb (d, g), ENR-Bi (e, h), and ENR-Sn (f, i) single crystals. (d)−(f) daylight; (g)−(i) 365 nm UV light.

by regulating their local environment. It is well-known that the PL of pure organic cations are closely related to their rigidity. The bulk assembly of emissive organic cations and metal−halogen anions can form a hybrid metal halide, which can provide the rigid frame caused by hydrogen bonds and $\pi−\pi$ interactions. Furthermore, in compounds, the flexibility of pure organic cations is decreased; thus, the tunable PL for pure organic cations is realized.[21−26] And thus, several functionalized metal halides are obtained by assembling pure organic cations with multifarious metal−halogen anions. Here, we reported three new hybrid metal halides, $(EnrofloH_2)Pb_2Cl_6\cdot H_2O$ (abbreviated as ENR-Pb), $(EnrofloH_2)BiCl_5\cdot Cl\cdot 2(H_2O)\cdot H_3O$ (abbreviated as ENR-Bi), and $(EnrofloH_2)SnCl_6\cdot H_2O$ (abbreviated as ENR-Sn). The theoretical calculation and experimental results indicated that the emissions of these three single crystal compounds come from the singlet state fluorescence emissions of $EnrofloH_2{}^{2+}$ organic cations. Interestingly, the fluorescence emissions of $EnrofloH_2{}^{2+}$ in these single crystal compounds have large differences, such as maximum emission wavelengths, full width at half-maximum (FWHM), Stokes shift, and PLQY due to the discrepant confined environment of the organic cations. In as-synthesized metal halides, the organic cations and metal−chloride anions are connected by hydrogen bonds, and the hydrogen-bond networks in the environment of organic cations enables enhancement of their rigid degree. Moreover, serried packing of $EnrofloH_2{}^{2+}$ in different hybrid metal halide can provide

stronger $\pi−\pi$ stacking interactions, which further improve the rigid degree of organic cations.[27] It is worth noting that there are both inter and intramolecular hydrogen bonds and $\pi−\pi$ interactions in ENR-Sn, the emission spectrum has the smallest FWHM with 40 nm and Stokes shift with 30 nm, and the PLQY of up to 19.23 %. As a result, organic−inorganic hybrid metal halides synthesized by emissive organic cations show better optical properties than single organic cations. Our work not only provides a series of new hybrid metal halide materials for future emerging optoelectronic applications but also provides an essential way to adjust the optical properties of the pure organic cations by rational assembly.

The crystallographic information files (CIF) of the as-synthesized single crystal compounds, ENR-Pb, ENR-Bi, and ENR-Sn, are demonstrated in the Supporting Information, and the main crystal data are shown in Table S1. The comparisons of experimental and calculated X-ray diffraction (XRD) patterns of ENR-Pb, ENR-Bi, and ENR-Sn single crystal compounds are demonstrated in Figure 2a−c. It is worth mentioning that there are some differences between the calculated and experimental XRD patterns due to the preferred crystallite orientation. The optical microscopic images of these as-synthesized metal halide single crystals under daylight and ultraviolet light (UV) are described in Figure 2d−i. All of the single crystals show the yellow colors in daylight. Under the excitation of 365 nm UV light, these three single crystals show the bright blue fluorescence. The ENR-Pb single crystal
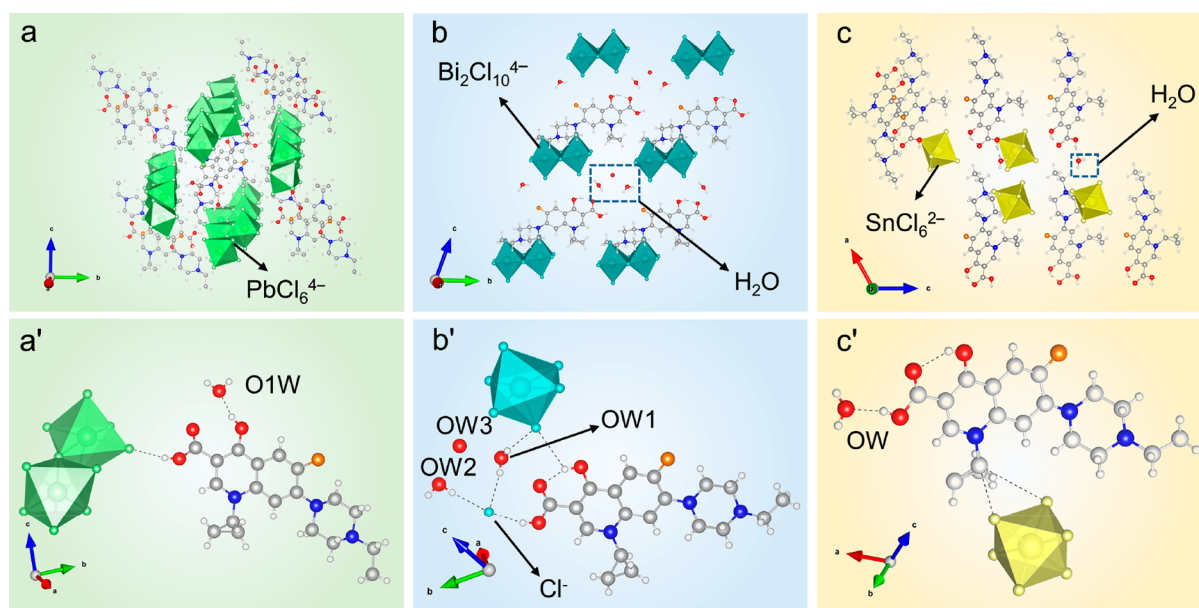
Figure 3. Crystal structure diagrams and asymmetric parts of unit cell structures of ENR-Pb (a, a′), ENR-Bi (b, b′), and ENR-Sn (c, c′) single crystals: $PbCl_6^{4-}$, green; $BiCl_6^{3-}$, cyan; $SnCl_6^{2-}$, yellow. Atoms: Pb, green; Bi, cyan; Sn, yellow; N, blue; O, red; F, orange; C, gray; H, white, and the color of Cl atoms are in agreement with the corresponding colors of metal−chloride anions.
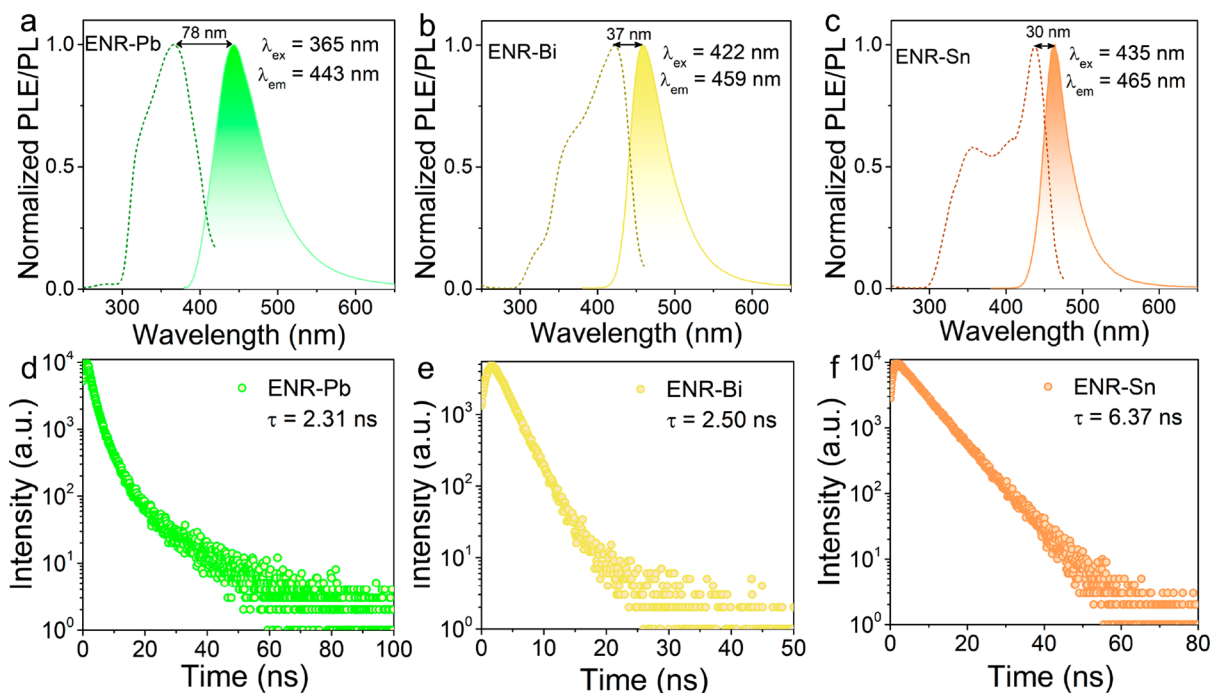

Figure 4. Normalized PL and PLE spectra of ENR-Pb (a), ENR-Bi (b), and ENR-Sn (c) single crystals at room temperature. The arrows in (a)−(c) show the Stokes shifts. Decay curves of ENR-Pb (d), ENR-Bi (e), and ENR-Sn (f) single crystals at room temperature.

crystallizes in centrosymmetric monoclinic space group $P2_1/c$. The asymmetric part contains one ion of $C_{19}H_{24}FN_3O_3^{2+}$ ($EnrofloH_2^{2+}$), two Pb^{2+} ions, six coordinated Cl^- ions, and one H_2O molecule (Figure 3a′). The main bond lengths are shown in Tables S2. Each Pb^{2+} ion is coordinated by six Cl^- ions and forms $PbCl_6^{4-}$ metal−chloride anions. It is of interest to note that the $PbCl_6^{4-}$ are connected by nodes-sharing, edge-sharing, and face-sharing, forming infinite double chain (Figure 3a). There are O−H···Cl, O−H···O, N−H···Cl, C−H···Cl, and C−H···O hydrogen bonds in the structure (Table S3), three of which are intramolecular hydrogen bonds. Intermolecular

hydrogen bonds form 3D net, which joints the $EnrofloH_2^{2+}$ cations with $PbCl_6^{4-}$ metal−chloride anions chains and H_2O molecules. The ENR-Bi single crystal crystallizes in triclinic space group $P\bar{1}$. The asymmetric part contains one $C_{19}H_{24}FN_3O_3^{2+}$ ($EnrofloH_2^{2+}$), one Bi^{3+} with five coordinated Cl^- ions and one Cl^- isolated ion, two H_2O molecules, and one H_3O^+ ion (Figure 3b′), so that the total charge of the unit cell is zero. The main bond lengths are shown in Tables S4. The Bi^{3+} ion is coordinated by six Cl^- ions and forms $BiCl_6^{3-}$ metal−chloride anions. The adjacent two octahedrons are linked with each other by edges forming a 0D block $Bi_2Cl_{10}^{4-}$

Table 1. Optical Properties of ENR-Pb (a), ENR-Bi (b), and ENR-Sn (c) Single Crystals

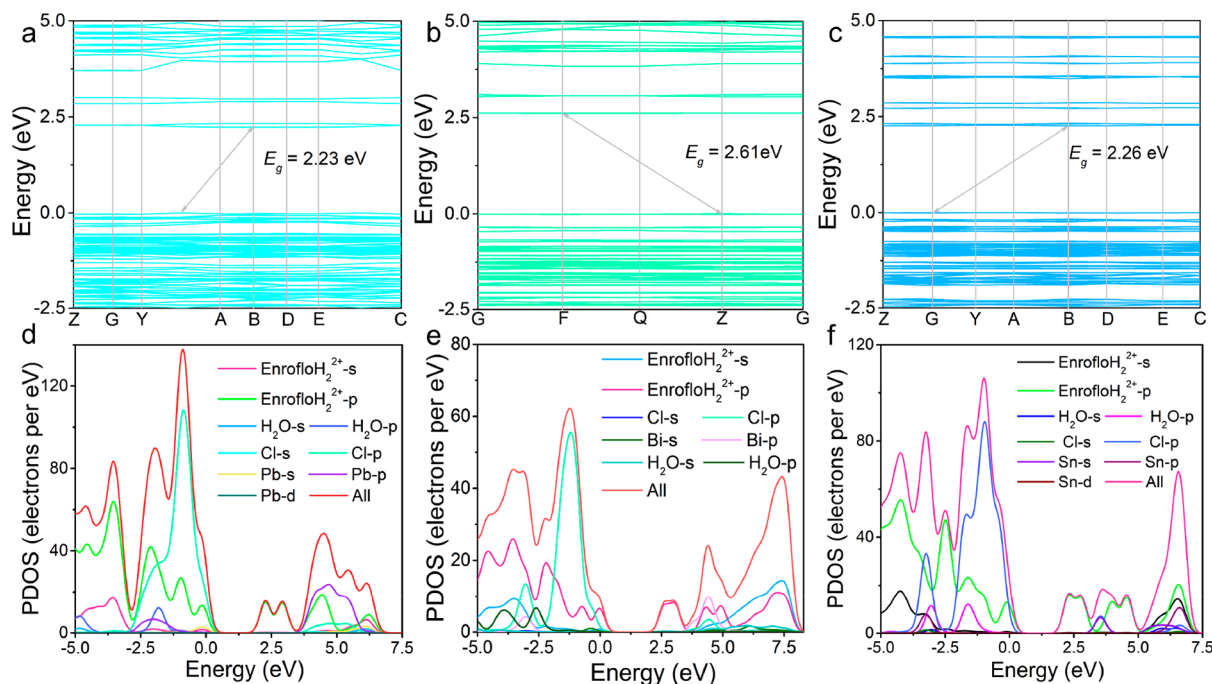| samples	excitation peak (nm)	emission peak (nm)	FWHM (nm)	Stokes shift (nm)	decay time (ns)	PLQY (%)
Enrofloxacin	430	544	129	114	2.77	<1
ENR-HCl	443	470	75	27	1.73	2.10
ENR-Pb	365	443	72	78	2.31	9.75
ENR-Bi	422	459	56	37	2.50	9.14
ENR-Sn	435	465	40	30	6.37	19.23

Figure 5. Calculated electronic band structure of ENR-Pb (a), ENR-Bi (b), and ENR-Sn (c) single crystals. Total and orbital-projected partial density of states of ENR-Pb (d), ENR-Bi (e), and ENR-Sn (f) single crystals calculated by DFT-PBE method.

(Figure 3b). There are O−H···Cl, O−H···O, N−H···Cl, C−H···Cl, and C−H···O hydrogen bonds in the structure (Table S5), three of which have intramolecular hydrogen bonds. Intermolecular hydrogen bonds form a 3D net, which joins the EnrofloH$_2^{2+}$ cations with BiCl$_6^{3-}$ metal−chloride anions, H$_2$O molecules and Cl$^-$ ions. The EnrofloH$_2$−Sn single crystal also crystallizes in centrosymmetric monoclinic space group $P2_1/c$. The asymmetric part contains one ion of C$_{19}$H$_{24}$FN$_3$O$_3^{2+}$ (EnrofloH$_2^{2+}$), one Sn^{4+} ion, six Cl$^-$ ions, and one H$_2$O molecule (Figure 3c′). The main bond lengths are shown in Tables S6. Each Sn^{4+} ion is coordinated by six Cl$^-$ ions and forms SnCl$_6^{2-}$ metal−chloride anions, which is isolated from each other (Figure 3c). There are O−H···Cl, O−H···O, N−H···Cl, C−H···Cl, and C−H···O hydrogen bonds in the structure (Table S7), three of which have intramolecular hydrogen bonds. Intermolecular H-bonds form 3D net, which joins the EnrofloH$_2^{2+}$ cations with SnCl$_6^{2-}$ metal−chloride anions and H$_2$O molecules.

Generally, the emissive organic cations exhibit fluorescence emission arising from singlet state with short lifetime or room-temperature phosphorescence (RTP) arising from triplet state with long lifetime.[28−32] The fluorescence spectra of Enrofloxacin powders are shown in Figure S1. Under 430 nm excitation, it shows the broadband yellow emission peaking at 544 nm with the PLQY of <1 %. The fluorescence lifetime of the emission is determined by time-resolved methods (Figure S2). The average lifetime of the emission at room temperature

is 2.77 ns based on double exponential-fitting. The room temperature optical properties of as-synthesized metal halides are investigated in detail, as shown in Figure 4. The photoluminescence excitation (PLE) spectra of all three compounds show broad excitation bands from 300−450 nm. Under the excitation at 365 and 422 nm, ENR-Pb and ENR-Bi single crystals show the blue emission peaking at 443 and 459 nm with the Stokes shift of 78 and 37 nm and a FWHM of 72 and 56 nm, respectively (Figure 4a). Under the excitation at 435 nm, the ENR-Sn single crystal shows the blue emissions peaking at 465 nm (Figure 4b,c) with the Stokes shift of 30 nm and a FWHM of 40 nm (Figure 4e,f). The lifetime of ENR-Sn at room temperature is 6.37 ns based on single exponential-fitting. Especially, the average lifetime of ENR-Pb and ENR-Bi at room temperature are 2.31 and 2.5 ns based on double exponential-fitting, respectively, which may be caused by effective nonradiative energy transfer. It is consistent with the observed low PLQYs of ENR-Pb and ENR-Bi single crystals. We attribute these blue emissions to the singlet state fluorescence emission of EnrofloH$_2^{2+}$ cations, because the Enrofloxacin in solution also shows the similar blue emissions.[20,33] As mentioned above, Enrofloxacin exists in the form of LH$_2^{2+}$ (divalent cation) in the strong acidic conditions, in which the maximum emission wavelength is located at 450 nm. When Enrofloxacin exists in the form of LH$^+$ (monovalent cation) under the pH condition of 2.45−4.23, the maximum emission wavelength is still at 450 nm.
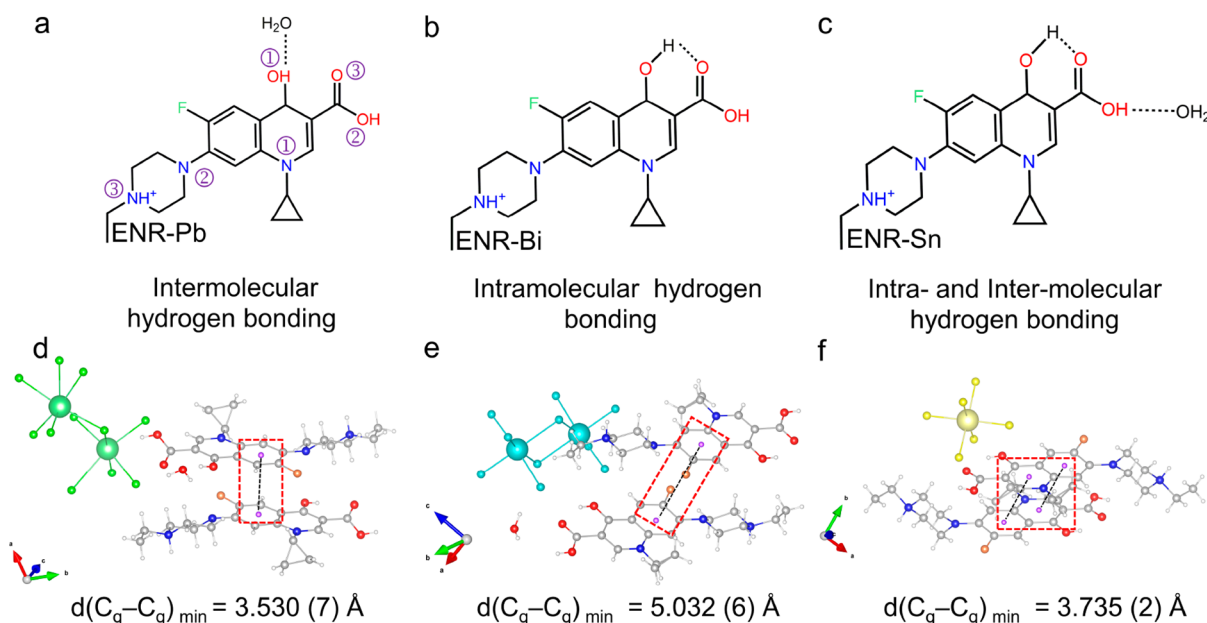
Figure 6. Chemical structure of EnrofloH$_2^{2+}$ cations in ENR-Pb (a), ENR-Bi (b), and ENR-Sn (c) single crystals. The dotted lines (a)−(c) show the type of hydrogen bonding. Layered stack of EnrofloH$_2^{2+}$ in ENR-Pb (a), ENR-Bi (b), and ENR-Sn (c) single crystals. The dotted lines (d)−(f) show the shortest distance of two adjacent benzene rings in EnrofloH$_2^{2+}$ cations.

When the pH value is larger than 4.23, Enrofloxacin exists in the form of L (bipolar), and the maximum emission wavelength gradually shifted to 445 nm with the decreased fluorescence intensity. When the pH value is more than 12.28, Enrofloxacin exists in the form of L$^-$ (anion), the maximum emission wavelength is still at 445 nm, but the fluorescence intensity decreased and nearly disappeared with the increase of the pH value.[33] One can conclude that the divalent cation species only exist in extremely acidic conditions. Therefore, we analyze the optical properties of Enrofloxacin in HCl solution with the concentration of 11−12 mol/L (ENR-HCl); the fluorescence spectra of ENR-HCl are shown in Figure S3. Under the excitation at 443 nm, ENR-HCl shows the blue emission peaking at 470 nm with the Stokes shift of 27 nm and a FWHM of 75 nm, and the PLQY of 2.11 %. The detailed optical properties of Enrofloxacin, ENR-HCl, and hybrid metal halides are summarized in Table 1. It is of interest to note that the PL properties of EnrofloH$_2^{2+}$ organic cations have significant distinctions in solution and in different single crystals, such as the maximum excitation and emission wavelength, FWHM, and PLQY. Especially, the PLQY of ENR-Sn single crystal reaches 19.73 %, and the FWHM of the corresponding emission peak is only 40 nm. We also analyze the effect of excitation wavelength on the fluorescence emission for these three single crystal compounds (Figures S5−S7). The emission wavelengths remain unchanged with the change of excitation wavelengths, indicating that there was only one luminescence center in these single crystal compounds.

To further verify the PL origin of these as-synthesized metal halides, we analyze the electronic band structures and density of states (DOS) of these three single crystal compounds by density functional theory (DFT). As shown in Figure 4, ENR-Pb, ENR-Bi, and ENR-Sn all have the indirect bandgaps with 2.23, 2.61, and 2.26 eV (Figure 5a−c), respectively. The valence band maximum (VBM) of these compounds are all made up of EnrofloH$_2^{2+}$-p and Cl-6p orbitals, and the

conduction band minimum (CBM) are all composed of EnrofloH$_2^{2+}$-p (Figure 5d,e), which indicated that the center metal ions have no contribution to the frontier orbital in these hybrid metal halides. In other words, the fluorescence emissions of all synthesized compounds come from the EnrofloH$_2^{2+}$ organic cations, which is consistent with observed optical characteristic. In addition, it also can be found from the synthesis processes of these compounds that all of the single crystal compounds are composed of protonated organic cations and metal−chloride anions. Therefore, the fluorescence emissions of these single crystal compounds belong to the corresponding organic cations with certain degree of protonation. Figure 6 shows the chemical structures of EnrofloH$_2^{2+}$ cations in ENR-Pb, ENR-Bi, and ENR-Sn, which are used to analyze the degree of protonation of Enrofloxacin in targeted compounds. The organic components of these single crystal compounds have the same degree of protonation, including 3-position nitrogen (N3) in the piperazinyl group and 1-position carbonyl oxygen (O1) in the quinoline ring (Figure 6a−c), which is similar to other ionic compounds composed of ciprofloxacin and Bi(III) chloride anions.[34,35] In neutral and acid solutions, according to the different pH conditions, the fluoroquinolones (FQ) might exist in four protonation species, namely, dication FQH$_2^{2+}$, cation FQH$^+$, zwitterion zFQ, and neutral species nFQ.[36] The FQH$_2^{2+}$ only exist in extremely acidic conditions, which is consistent with the synthesized conditions of these three compounds in acid conditions with the concentration of HCl solution of 11−12 mol/L. In addition, FQH$_2^{2+}$ can be protonated either at the piperazine ring[37,38] or at carbonyl oxygen (O1) or even through the atom of pyridone ring (N1).[39] The results of the DFT calculation showed that the FQH$_2^{2+}$-O1 form is the most stable isomer in the gas phase and in water.[36] These results are also consistent with the observed protonation forms of EnrofloH$_2^{2+}$ cations in our synthesized compounds.
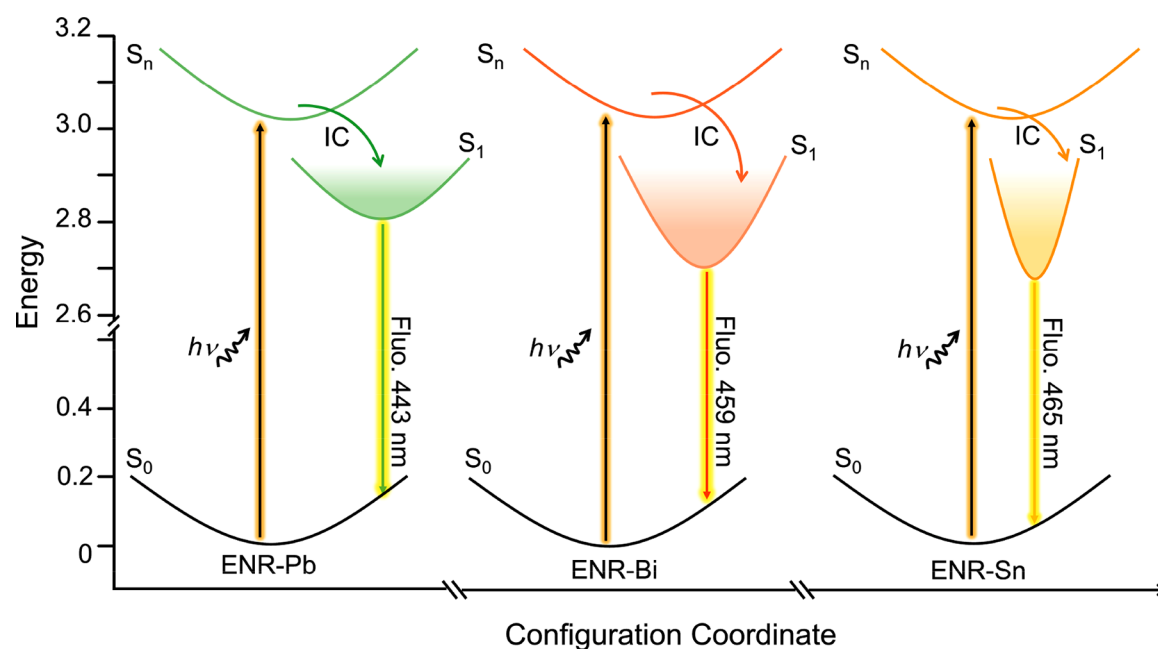
Figure 7. Energy level diagram of ENR-Pb (a), ENR-Bi (b), and ENR-Sn (c) single crystals. The S_n represent the high energy singlet states, the S_1 represent the low energy singlet state, the S_0 represent the ground state, and the IC represent the internal conversion.

Although Enrofloxacin has the same degree and form of protonation in these three compounds, the optical properties of protonated organic cations in these as-synthesized metal halides are significantly discrepant. As shown in Table 1, the maximum emission wavelength of these as-synthesized metal halides is red-shifted from 443 to 459 to 465 nm by changing metal−chloride anions from $Pb_2Cl_6^{2−}$ to $Bi_2Cl_{10}^{4−}$ to $SnCl_6^{2−}$. Moreover, the PL of ENR-Sn has the smallest Stokes shift of 30 nm and the FWHM of the corresponding emission peak is low to 40 nm and the PLQY is up to 19.23 %. One can conclude that under the same protonation form, the other factors should be involved, which greatly affect the fluorescence emissions of $EnrfloH_2^{2+}$ in synthesized single crystal compounds. As mentioned above, the PL of emissive organic cation is greatly affected by their local environment. The inter- and intramolecular hydrogen bonds and intermolecular π stacking interactions can form a more restraining effect and improve the rigid degree of organic cations, causing the red shift or blue shift of the spectrum and the variation of FWHM of corresponding emission peak. There are both inter- and intramolecular hydrogen bonds in three single crystal compounds. The intermolecular hydrogen bonds joint the $EnrfloH_2^{2+}$ with metal−chloride anions forming a 3D net, enhancing the rigid degree of $EnrfloH_2^{2+}$. Differently, in ENR-Pb, the proton of the carbonyl bound oxygen (O1) prefers to combine with the oxygen in isolated H_2O molecule rather than the carboxyl group bound oxygen (O3), forming an intermolecular hydrogen bond (Figure 6a). Conversely, in ENR-Bi, the proton of the carbonyl bound oxygen (O1) is combined with carboxyl group bound oxygen (O3), forming an intramolecular hydrogen bond (Figure 6b). Moreover, both intra- and inter- molecular hydrogen bonds are observed in ENR-Sn (Figure 6c), which come from the combination of the proton of the carboxyl group bound oxygen (O2) and oxygen in an isolated H_2O molecule. In addition to hydrogen bond interactions, π−π stacking interactions also play an important role in improving the rigidity of $EnrfloH_2^{2+}$ cations. Generally,

the organic cations in solution have more considerable flexibility. However, when liquid organic cations are transformed into solids forming highly ordered crystals, which have decreased flexibility. Furthermore, the denser packing of $EnrfloH_2^{2+}$ cations in single crystal compounds significantly reduces their flexibility due to π−π stacking interactions. Figure 6d−f shows the crystal packing of $EnrfloH_2^{2+}$ cations in these single crystal compounds. $EnrfloH_2^{2+}$ cations show the two infinite stacks (Figure 6d), and the offset face-to-face π−π stacking of phenyl rings are observed in the ENR-Pb compound, here the shortest distance between adjacent phenyl rings is 3.530 (7) Å. The $EnrfloH_2^{2+}$ cations also show the layered stack and the shortest distances between adjacent phenyl rings are 5.032 (6) Å in the ENR-Bi compound (Figure 6e), which are greater than the 4 Å,[40] so there are no π−π stacking interactions. Moreover, $EnrfloH_2^{2+}$ cations in ENR-Sn are stacked in layers, and adjacent layers are arranged vertically. The phenyl rings in $EnrfloH_2^{2+}$ cations show the offset face-to-face π−π stacking (Figure 6f), and the shortest distances between adjacent phenyl rings are 3.735 (2) Å. The detailed parameters of the π−π interactions in ENR-Pb and ENR-Sn single crystal compounds are listed in Table S8. The energy level diagrams of ENR-Pb, ENR-Bi, and ENR-Sn single crystal compounds are shown in Figure 7. Under the excitation at UV light, the ground state electrons are excited to a high energy singlet state (S_n), which undergoes the internal conversion (IC) to the lower energy singlet state (S_1) and then returns to ground state (S_0) to generate Stokes-shifted emissions with nanosecond decay times. However, due to the diverse local environment, the optical properties of $EnrfloH_2^{2+}$ cations in these three single crystal compounds are different. Thus, because of the coupling effect of hydrogen bonds and π−π stacking interactions, the emission of $EnrfloH_2^{2+}$ cations in ENR-Sn shows the smallest Stokes shift of 30 nm and the FWHM of the corresponding emission peak is low to 40 nm and the PLQY of up to 19.23 % with the best performance in the studied series.

In summary, we demonstrated an all-purpose strategy for modulating the optical properties of emissive organic cations by assembling them with metal−chloride anions. The single crystal bulk assembly of EnrofloH$_2^{2+}$ organic cation and different metal−chloride anions (Pb$_2$Cl$_6^{2-}$, Bi$_2$Cl$_{10}^{4-}$, SnCl$_6^{2-}$) can draw into additional interactions, improve the optical properties of EnrofloH$_2^{2+}$ organic cation, including modified excitation and emission wavelength, FWHM, and PLQY. The local structures and optical properties studies indicated that the hydrogen bond and π−π interactions can provide the rigid environment for the organic cation, which decrease the flexibility of the organic cation. Thus, the fluorescence emissions of the EnrofloH$_2^{2+}$ organic cation in hybrid metal halides have wide differences compared with pure organic cations in solutions. Our work not only demonstrates the role of metal−chloride anions in photoluminescence modulation of emissive organic cations in hybrid metal halides materials for future emerging optoelectronic applications but also provides a fundamental way for designing multifarious optical functional materials.

ASSOCIATED CONTENT

Supporting Information

The Supporting Information is available free of charge at https://pubs.acs.org/doi/10.1021/acs.jpclett.1c00182.

> Experimental section, Figures S1−S7 showing excitation and emission spectra, decay curves, and Tables S1−S8 providing main parameters of single crystal structure and the π−π interactions in ENR-Pb, ENR-Bi, and ENR-Sn single crystals (PDF)

> Crystallographic information of (EnrofloH$_2$)Pb$_2$Cl$_6$·H$_2$O (CIF)

> Crystallographic information of (EnrofloH$_2$)BiCl$_5$·Cl·2(H$_2$O)·H$_3$O (CIF)

> Crystallographic information of (EnrofloH$_2$)SnCl$_6$·H$_2$O (CIF)

AUTHOR INFORMATION

Corresponding Author

Zhiguo Xia − *The State Key Laboratory of Luminescent Materials and Devices, Guangdong Provincial Key Laboratory of Fiber Laser Materials and Applied Techniques, School of Materials Science and Technology, South China University of Technology, Guangzhou 510640, PR China;* orcid.org/0000-0002-9670-3223; Email: xiazg@scut.edu.cn

Authors

Binbin Su − *The State Key Laboratory of Luminescent Materials and Devices, Guangdong Provincial Key Laboratory of Fiber Laser Materials and Applied Techniques, School of Materials Science and Technology, South China University of Technology, Guangzhou 510640, PR China*

Gaomin Song − *Technical Institute of Physics and Chemistry, University of Chinese Academy of Sciences, Beijing 100190, China;* orcid.org/0000-0001-5535-0188

Maxim S. Molokeev − *Laboratory of Crystal Physics, Kirensky Institute of Physics, Federal Research Center KSC SB RAS, Krasnoyarsk 660036, Russia; Siberian Federal University, Krasnoyarsk 660041, Russia; Research and Development Department, Kemerovo State University, Kemerovo 650000, Russia;* orcid.org/0000-0002-8297-0945

Nicolay N. Golovnev − *Siberian Federal University, Krasnoyarsk 660041, Russia*

Maxim K. Lesnikov − *Siberian Federal University, Krasnoyarsk 660041, Russia*

Zheshuai Lin − *Technical Institute of Physics and Chemistry, University of Chinese Academy of Sciences, Beijing 100190, China; Center of Materials Science and Optoelectronics Engineering, University of the Chinese Academy of Sciences, Beijing 100049, China;* orcid.org/0000-0002-9829-9893

Complete contact information is available at:
https://pubs.acs.org/10.1021/acs.jpclett.1c00182

Author Contributions

#B.S. and G.S. contributed equally to this work.

Notes

The authors declare no competing financial interest.

ACKNOWLEDGMENTS

REFERENCES

(1) Jung, M.; Ji, S. G.; Kim, G.; Seok, S. I. Perovskite Precursor Solution Chemistry: from Fundamentals to Photovoltaic Applications. *Chem. Soc. Rev.* **2019**, *48*, 2011−2038.

(2) Zhao, Y. X.; Zhu, K. Organic-Inorganic Hybrid Lead Halide Perovskites for Optoelectronic and Electronic Applications. *Chem. Soc. Rev.* **2016**, *45*, 655−89.

(3) Li, M. Z.; Xia, Z. G. Recent Progress of Zero-dimensional Luminescent Metal Halides. *Chem. Soc. Rev.* **2021**, DOI: 10.1039/D0CS00779J.

(4) Zhou, G. J.; Su, B. B.; Huang, J. L.; Zhang, Q. Y.; Xia, Z. G. Broad-Band Emission in Metal Halide Perovskites: Mechanism, Materials, and Applications. *Mater. Sci. Eng., R* **2020**, *141*, 100548.

(5) Cao, F. R.; Tian, W.; Wang, M.; Wang, M.; Li, L. Stability Enhancement of Lead-Free CsSnI$_3$ Perovskite Photodetector with Reductive Ascorbic Acid Additive. *InfoMat* **2020**, *2*, 577−584.

(6) Zhu, P. C.; Zhu, J. Low-Dimensional Metal Halide Perovskites and Related Optoelectronic Applications. *InfoMat* **2020**, *2*, 341−378.

(7) Hao, D. D.; Zou, J.; Huang, J. Recent Developments in Flexible Photodetectors Based on Metal Halide Perovskite. *InfoMat* **2020**, *2*, 139−169.

(8) Cortecchia, D.; Neutzner, S.; Srimath Kandada, A. R.; Mosconi, E.; Meggiolaro, D.; De Angelis, F.; Soci, C.; Petrozza, A. Broadband Emission in Two-dimensional Hybrid Perovskites: the Role of Structural Deformation. *J. Am. Chem. Soc.* **2017**, *139*, 39−42.

(9) Smith, M. D.; Karunadasa, H. I. White-Light Emission from Layered Halide Perovskites. *Acc. Chem. Res.* **2018**, *51*, 619−627.

(10) Dohner, E. R.; Jaffe, A.; Bradshaw, L. R.; Karunadasa, H. I. Intrinsic White-Light Emission from Layered Hybrid Perovskites. *J. Am. Chem. Soc.* **2014**, *136*, 13154−13157.

(11) Krishnamurthy, S.; Naphade, R.; Mir, W. J.; Gosavi, S.; Chakraborty, S.; Vaidhyanathan, R.; Ogale, S. Molecular and Self-trapped Excitonic Contributions to The Broadband Luminescence in Diamine-Based Low-dimensional Hybrid Perovskite systems. *Adv. Opt. Mater.* **2018**, *6*, 1800751.

(12) Zhuang, Z.; Peng, C. D.; Zhang, G. Y.; Yang, H. M.; Yin, J. L.; Fei, H. H. Intrinsic Broadband White-Light Emission from Ultra-

stable, Cationic Lead Halide Layered Materials. *Angew. Chem., Int. Ed.* **2017**, *56*, 14411−14416.

(13) Barkaoui, H.; Abid, H.; Yangui, A.; Triki, S.; Boukheddaden, K.; Abid, Y. Yellowish White-Light Emission Involving Resonant Energy Transfer in a New One-dimensional Hybrid Material: $(C_9H_{10}N_2)$-$PbCl_4$. *J. Phys. Chem. C* **2018**, *122*, 24253−24261.

(14) Xu, L. J.; Plaviak, A.; Lin, X. S.; Worku, M.; He, Q.; Chaaban, M.; Kim, B. J.; Ma, B. W. Metal Halide Regulated Photophysical Turning of Zero-Dimensional Organic Metal Halide Hybrids: from Efficient Phosphorescence to Ultralong Afterglow. *Angew. Chem., Int. Ed.* **2020**, *59*, 23067−23071.

(15) Yangui, A.; Roccanova, R.; McWhorter, T. M.; Wu, Y.; Du, M. H.; Saparov, B. Hybrid Organic-Inorganic Halides $(C_5H_7N_2)_2MBr_4$ (M = Hg, Zn) with High Color Rendering Index and High-Efficiency White-Light Emission. *Chem. Mater.* **2019**, *31*, 2983−2991.

(16) Turel, I. The Interactions of Metal Ions with Quinolone Antibacterial Agents. *Coord. Chem. Rev.* **2002**, *232*, 27−47.

(17) Yan, W.; Hu, S.; Jing, C. Y. Enrofloxacin Sorption on Smectite Clays: Effects of pH, Cations, and Humic Acid. *J. Colloid Interface Sci.* **2012**, *372*, 141−147.

(18) Wierzchowski, J.; Sepioł, J.; Sulikowski, D.; Kierdaszuk, B.; Shugar, D. Fluorescence Emission Properties of 8-azaxanthine and Its N-alkyl Derivatives: Excited-State Proton Transfer, and Potential Applications in Enzymology. *J. Photochem. Photobiol., A* **2006**, *179*, 276−282.

(19) Zhang, W. S.; Tang, B.; Liu, X.; Liu, Y. Y.; Xu, K. H.; Ma, J. P.; Tong, L. L.; Yang, G. W. A Highly Sensitive Acidic pH Fluorescent Probe and Its Application to HepG2 Cells. *Analyst* **2009**, *134*, 367−371.

(20) Drakopoulos, A. I.; Ioannou, P. C. Spectrofluorimetric Study of the Acid-Base Equilibria and Complexation Behavior of the Fluoroquinolone Antibiotics Ofloxacin, Norfloxacin, Ciprofloxacin and Pefloxacin in Aqueous Solution. *Anal. Chim. Acta* **1997**, *354*, 197−204.

(21) Hu, H.; Meier, F.; Zhao, D.; Abe, Y.; Gao, Y.; Chen, B.; Salim, T.; Chia, E. E. M.; Qiao, X.; Deibel, C.; Lam, Y. M. Efficient Room-Temperature Phosphorescence from Organic-Inorganic Hybrid Perovskites by Molecular Engineering. *Adv. Mater.* **2018**, *30*, 1707621.

(22) Hamzehpoor, E.; Perepichka, D. F. Crystal Engineering of Room Temperature Phosphorescence in Organic Solids. *Angew. Chem., Int. Ed.* **2020**, *59*, 9977−9981.

(23) Cariati, E.; Forni, A.; Lucenti, E.; Marinotto, D.; Previtali, A.; Righetto, S.; Botta, C.; Bold, V.; Kravtsov, V.; Fonari, M. S. Extrinsic Heavy Metal Atom Effect on the Solid-State Room Temperature Phosphorescence of Cyclic Triimidazole. *Chem. - Asian J.* **2019**, *14*, 853−858.

(24) Yuan, M. S.; Wang, D. E.; Xue, P. C.; Wang, W. J.; Wang, J. C.; Tu, Q.; Liu, Z. Q.; Liu, Y.; Zhang, Y. R.; Wang, J. Y. Fluorenone Organic Crystals: Two-Color Luminescence Switching and Reversible Phase Transformations between *π-π* Stacking-Directed Packing and Hydrogen Bond-Directed Packing. *Chem. Mater.* **2014**, *26*, 2467−2477.

(25) Cui, B. B.; Han, Y.; Huang, B.; Zhao, Y.; Wu, X.; Liu, L.; Cao, G.; Du, Q.; Liu, N.; Zou, W.; Sun, M.; Wang, L.; Liu, X.; Wang, J.; Zhou, H.; Chen, Q. Locally Collective Hydrogen Bonding Isolates Lead Octahedra for White Emission Improvement. *Nat. Commun.* **2019**, *10*, 5190.

(26) Lin, H. R.; Zhou, C. K.; Chaaban, M.; Xu, L. J.; Zhou, Y.; Neu, J.; Worku, M.; Berkwits, E.; He, Q. Q.; Lee, S.; Lin, X. S.; Siegrist, T.; Du, M. H.; Ma, B. W. Bulk Assembly of Zero-Dimensional Organic Lead Bromide Hybrid with Efficient Blue Emission. *ACS Mater. Lett.* **2019**, *1*, 594−598.

(27) Su, B. B.; Song, G. M.; Molokeev, M. S.; Lin, Z. S.; Xia, Z. G. Synthesis, Crystal Structure and Green Luminescence in Zero-Dimensional Tin Halide $(C_8H_{14}N_2)_2SnBr_6$. *Inorg. Chem.* **2020**, *59*, 9962−9968.

(28) Xie, Z.; Chen, C.; Xu, S.; Li, J.; Zhang, Y.; Liu, S.; Xu, J.; Chi, Z. White-Light Emission Strategy of a Single Organic Compound with Aggregation-Induced Emission and Delayed Fluorescence Properties. *Angew. Chem., Int. Ed.* **2015**, *54*, 7181−4.

(29) Yang, Q. Y.; Lehn, J. M. Bright White-Light Emission from a Single Organic Compound in the Solid State. *Angew. Chem., Int. Ed.* **2014**, *53*, 4572−7.

(30) Li, D.; Hu, W.; Wang, J.; Zhang, Q.; Cao, X. M.; Ma, X.; Tian, H. White-Light Emission from a Single Organic Compound with Unique Self-Folded Conformation and Multistimuli Responsiveness. *Chem. Sci.* **2018**, *9*, 5709−5715.

(31) Mu, Y.; Yang, Z.; Chen, J.; Yang, Z.; Li, W.; Tan, X.; Mao, Z.; Yu, T.; Zhao, J.; Zheng, S.; Liu, S.; Zhang, Y.; Chi, Z.; Xu, J.; Aldred, M. P. Mechano-Induced Persistent Room-Temperature Phosphorescence from Purely Organic Molecules. *Chem. Sci.* **2018**, *9*, 3782−3787.

(32) He, Z.; Zhao, W.; Lam, J. W. Y.; Peng, Q.; Ma, H.; Liang, G.; Shuai, Z.; Tang, B. Z. White Light Emission from a Single Organic Molecule with Dual Phosphorescence at Room Temperature. *Nat. Commun.* **2017**, *8*, 416.

(33) Ma, L. H.; Liu, B. S.; Wang, C. D.; Zhang, H. C.; Cheng, X. The Investigation of Fluorescence Spectra and Fluorescence Quantum Yield of Enrofloxacin. *J. Chem. Environ. Biol. Eng.* **2018**, *2*, 11−16.

(34) Turel, I.; Leban, I.; Bukovec, N. Crystal Structure and Characterization of the Bismuth(III) Compound with Quinolone Family Member (ciprofloxacin). Antibacterial Study. *J. Inorg. Biochem.* **1997**, *66*, 241−245.

(35) Turel, I.; Leban, I.; Klintschar, G.; Bukovec, N.; Zalar, S. Synthesis, Crystal Structure, and Characterization of Two Metal-Quinolone Compounds. *J. Inorg. Biochem.* **1997**, *66*, 77−82.

(36) Nurchi, V.; Crisponi, G.; Lachowicz, J. I.; Zoroddu, M.; Peana, M.; Medici, S.; Veclani, D.; Tolazzi, M.; Melchior, A. Fluoroquinolones: A Micro-Species Equilibrium in the Protonation of Amphoteric Compounds. *Eur. J. Pharm. Sci.* **2016**, *93*, 380−91.

(37) Lin, C. E.; Deng, Y. J.; Liao, W. S.; Sun, S. W.; Lin, W. Y.; Chen, C. C. Electrophoretic Behavior and pKa Determination of Quinolones with a Piperazinyl Substituent by Capillary Zone Electrophoresis. *J. Chromatogr. A* **2004**, *1051*, 283−290.

(38) Rusu, A.; Toth, G.; Szocs, L.; Kokosi, J.; Kraszni, M.; Gyeresi, A.; Noszal, B. Triprotic Site-Specific Acid-Base Equilibria and Related Properties of Fluoroquinolone Antibacterials. *J. Pharm. Biomed. Anal.* **2012**, *66*, 50−57.

(39) Buckingham, D.; Clark, C.; Nangia, A. The Acidity of Norfloxacin. *Aust. J. Chem.* **1990**, *43*, 301−309.

(40) Sinnokrot, M. O.; Valeev, E. F.; Sherrill, C. D. Estimates of the ab Initio Limit for pi-pi Interactions: the Benzene Dimer. *J. Am. Chem. Soc.* **2002**, *124*, 10887−93.